AGU ADVANCING EARTH AND SPACE SCIENCE

JGR Atmospheres

RESEARCH ARTICLE
10.1029/2020JD033894

Key Points:
- A total of 70% of China's land area suffered from the dry-wet abrupt alternation events at least once during 1975–2004
- The dry-wet abrupt alternation events are projected to occur more frequently with greater intensity in the North China Plain
- The 95th percentile rainfall event contributes most to the wet-dry alternation event for most climate divisions of China

Supporting Information:
- Supporting Information S1

Correspondence to:
S. Wang,
shuo.s.wang@polyu.edu.hk

Citation:
Chen, H., Wang, S., Zhu, J., & Zhang, B. (2020). Projected changes in abrupt shifts between dry and wet extremes over China through an ensemble of regional climate model simulations. *Journal of Geophysical Research: Atmospheres*, *125*, e2020JD033894. https://doi.org/10.1029/2020JD033894

Received 12 SEP 2020
Accepted 17 NOV 2020
Accepted article online 21 NOV 2020

Author Contributions:
Conceptualization: S. Wang
Data curation: H. Chen
Formal analysis: H. Chen, B. Zhang
Funding acquisition: S. Wang
Investigation: S. Wang
Methodology: H. Chen, S. Wang
Project administration: S. Wang
Resources: S. Wang, J. Zhu
Supervision: S. Wang
Validation: H. Chen, J. Zhu, B. Zhang
Visualization: H. Chen
Writing - original draft: H. Chen
Writing – review & editing: S. Wang

Projected Changes in Abrupt Shifts Between Dry and Wet Extremes Over China Through an Ensemble of Regional Climate Model Simulations

H. Chen[1], S. Wang[1,2], J. Zhu[3], and B. Zhang[1]

[1]Department of Land Surveying and Geo-Informatics, The Hong Kong Polytechnic University, Hong Kong, China, [2]Hong Kong Polytechnic University Shenzhen Research Institute, Shenzhen, China, [3]School of Geography and Planning, Sun Yat-sen University, Guangzhou, China

Abstract The dry-wet abrupt alternation (DWAA) event, which is defined as the phenomenon of dry (or wet) spells abruptly following wet (or dry) spells, magnifies the influence of individual wet and dry events. The dynamic evolution of DWAA events has not been studied for different climate zones of China that is particularly susceptible to dry and wet extremes. This study explores the future changes in the abrupt alternations between dry and wet extremes across 10 climate divisions of China, with a thorough assessment of dry and wet conditions using the Standardized Precipitation Evapotranspiration Index (SPEI). We take advantage of an ensemble of regional climate model simulations including the Providing Regional Climate Impacts for Studies (PRECIS) experiment and five CORDEX East Asia experiments to produce high-resolution climate information for a baseline period of 1975–2004 and a future period of 2069–2098. Our findings disclose that a total of 70% of China's land area suffered from the DWAA events at least once during 1975–2004. The wet-dry alternation event is projected to become more frequent in summer, and a prominent increase in the number of dry-wet alternation events is expected to occur in spring over most parts of China. Moreover, an increasing number of DWAA events with intensified magnitude is projected to strike the North China Plain dominated by warm temperature and humid zone, which is the most densely populated region of the country and is also the largest agriculture production area. Our findings also reveal a strong positive correlation between DWAA and heavy rainfall. The 95th percentile rainfall event contributes most to the wet-dry alternation event for most climate divisions of China.

Plain Language Summary The emerging disaster of dry-wet abrupt alternation (DWAA) has been receiving increasing attention due to its compound effects on agricultural production and socioeconomic development. Since China is exposed to dry and wet hydrological extremes as well as their interconnections, a first attempt is made in this study to explore the historical evolution and the future change in the abrupt shifts between dry and wet extremes for different climate divisions of China. Our findings reveal that a total of 70% of China's land area suffered from DWAA events at least once from 1975 to 2004. More importantly, the DWAA is expected to occur more frequently and intense by the end of the 21st century, especially for the North China Plain which is the most densely populated region of the country and is also the largest agricultural production area. Moreover, the summertime wet-dry alternation is expected to become more frequent for most climate divisions of China, while the dry-wet alternation event is projected to occur more frequently in spring over East China. These findings provide meaningful insights into the development of adaptation strategies for enhancing society's resilience to compound extremes in a changing climate.

1. Introduction

Dry-wet abrupt alternation (DWAA) has raised increasing attention from the hydroclimate community owing to the compound impacts of drought and pluvial events followed by each other (Christian et al., 2015; Espinoza et al., 2012; Hastenrath et al., 2010; Yoon et al., 2018). Although droughts (or dry spells) and pluvials (or wet spells) are usually treated separately due to different spatial-temporal features and the use of different metrics, both of them are highly related to precipitation anomalies. In fact, droughts and pluvials are interconnected and dominated by the similar hydrological processes and atmospheric dynamics (He & Sheffield, 2020). It is thus desired to detect the transition between droughts and pluvials in order to

advance our understanding of physical mechanisms causing the consecutive occurrence of dry and wet extremes.

Although pluvials can sometimes alleviate drought conditions, the abrupt alternation between droughts and pluvials may cause substantial damage to properties and losses of human lives when pluvials lead to severe floods. Thus, the consecutive occurrence of droughts and pluvials has received increasing attention over the past decade. For example, Dong et al. (2011) investigated the 2006 drought and the 2007 pluvial in the Southern Great Plains. Yoon et al. (2018) presented that Texas experienced the worst drought during 2011–2015, which was suddenly ended by a heavy precipitation event in spring 2015. The following pluvial event caused flash floods, thereby devastating the consequences of the previous drought event which already caused substantial damage. There is also plenty of evidence to show that the consecutive occurrence of drought and pluvial events can have a greater influence on agricultural production and economic losses than individual hydrological extremes (Chen, Wang, & Wang, 2020; Darenova et al., 2017; Handwerger et al., 2019; He & Sheffield, 2020).

China is exposed to frequent hydrological extremes, including droughts (Liu et al., 2019; Zhang et al., 2020), floods (Wang & Gu, 2016; Zong & Chen, 2000), and the co-occurrence of droughts and floods (Long et al., 2014; Ma et al., 2019). The dramatic switch between droughts and floods was also observed in some regions of China (Du et al., 2013; Feng et al., 2014; Ma et al., 2019). Wu et al. (2006) proposed a drought-flood coexistence index to investigate the co-occurrence of droughts and floods in summer from 1957 to 2000 in the Yangtze River Basin of South China. Yan et al. (2013) investigated an extreme rainfall occurrence after a drought period in the Huang-Huai-Hai River Basin of North China based on station data from 1961 to 2011. Shan et al. (2018) analyzed the spatial-temporal characteristics of the transition between dry spells and wet spells in summer, in the Yangtze River Basin, based on station data from 1960 to 2015. Ji et al. (2018) investigated the hazard levels of sudden alternation between droughts and floods in the Huai River Basin of Central East China over the period from 1955 to 2010. Previous studies mainly focus on the Yangtze-Huai River Basin with an emphasis on the transition of summertime drought and flood events. Due to complex geographical features and diverse climatic conditions over China, there is a lack of a thorough assessment of DWAA events across different seasons and climate zones of China.

In addition, it is recognized that the changing climate has contributed to a considerable increase in the frequency and magnitude of hydrological extremes (Carvalho & Wang, 2020; Chen, Wang, Wang, & Zhu, 2020; He & Sheffield, 2020; Wang et al., 2018; Wang & Wang, 2019; Zhang et al., 2019). The intensification of the hydrological cycle is expected to amplify the temporal and spatial heterogeneity of precipitation under global warming (Madakumbura et al., 2019), by increasing the intensity of heavy rainfall at the expense of light to moderate rainfall (Wang et al., 2017). This can result in an amplification of the fluctuations between periods of heavy precipitation (wet spells) and low precipitation (dry spells) (Annamalai et al., 2001; Giorgi et al., 2011; Singh et al., 2014). Therefore, it is necessary to project future changes in the abrupt alternation between dry and wet spells in a changing climate so as to identify the most vulnerable regions. Based on global climate model simulations, Swain et al. (2018) disclosed that a 25% to 100% increase in dry-to-wet events is projected over California at the end of the 21st century as a result of anthropogenic forcing. Projected future changes in the swing between dry and wet extremes, however, remain inadequate, especially for China with unique climate characteristics and complex geographical features. Thus, it is desired to conduct a comprehensive and reliable assessment and projection of the rapid transition between dry and wet extremes in China, which can facilitate the development of adaptation strategies and to strengthen society's resilience to future compound extreme events.

The aim of this paper is to explore the dynamic evolution of DWAA events and potential causes from both historical and future perspectives for 10 climate divisions of China. The high-resolution climate information will be produced through an ensemble of regional climate model simulations, including the Providing Regional Climate Impacts for Studies (PRECIS) experiment and five CORDEX East Asia experiments for a baseline period from 1975 to 2004 and a future period from 2069 and 2098 under the business-as-usual Representative Concentration Pathway 8.5 (RCP8.5). The standardized precipitation evapotranspiration index (SPEI) will be used to characterize dry and wet extremes as well as the rapid transition between extremes at each grid cell. Moreover, the underlying interrelationships between two different types of

DWAA and heavy rainfall with different intensities as well as potential evapotranspiration (PET) will be examined thoroughly to further explore the mechanisms that trigger the occurrence of DWAA.

This paper is organized as follows. Section 2 will introduce the study region, data sets, models, and heavy rainfall indices as well as the definition of DWAA. In section 3, the temporal and spatial evolution of heavy rainfall events will be examined for the historical and future periods, the historical DWAA events will be reproduced, the future changes of DWAA events will be projected, and the interrelationships between various DWAA events and heavy rainfall with different intensities as well as PET will be revealed for 10 climate regions of China. In section 4, the primary novelty of this work and the key findings will be highlighted.

2. Study Region, Data Sets, and Methods

2.1. Study Region

China is prone to experiencing a great number of droughts and floods due to its complex topography and climatic features (Yan et al., 2013; Zhang et al., 2020). China's average altitude is less than 100 m in the east and raises to over 4,000 m in the west (Figure 1b). The mainland consists of mountains (33%), plateaus (25%), valleys (19%), plains (12%), and hills (10%). Most areas of South China are dominated by the East Asia Summer Monsoon (EASM) climate which has a feature of high-frequency abnormal weather and climate extremes (Tang et al., 2016). By contrast, the mainland is affected by the dry cold air masses from Siberia in winter. The features related to continental climates can be characterized with hotter summer, colder winter, and more varied annual temperatures than other parts of the world with similar latitudes (Yang et al., 2008). The monsoon climate, therefore, tends to be dominant, with a marked change of wind directions between winter and summer as well as seasonal variations of precipitation depending on the advance and retreat of monsoon in China (Yang et al., 2008). Mountains and plateaus prevent the moisture from the EASM penetrating into Northwest China, thereby leading to low moisture there. However, the instability of monsoonal precipitation has a substantial influence on the frequency and magnitude of hydrological extremes such as droughts and floods (Wang et al., 2014).

China has continental and monsoon climates, and the region of the mainland can be divided into 10 climate divisions, as shown in Figure 1a. The average annual temperature increases from south to north including warm and cool temperatures, except for the southwestern part located on a high plateau with cool temperature due to the high-altitude effect (Figure 1c). The average annual precipitation shows an increasing trend from northwest to southeast (Figure 1d). The average annual PET shows lower values in Tibet and the northernmost part but higher values in south and northwest (Figure 1e). The temporal distribution of annual precipitation is not uniform, with more than 60% of annual precipitation occurring in late spring and summer (Du et al., 2013). And heavy rainfall is mostly concentrated in Southeast China. The uneven distribution of the interannual precipitation results in an increased risk of droughts and floods across different regions of China, thus further leading to the occurrence of a dramatic swing between dry and wet extremes.

2.2. Data Sets

The Climate Research Unit (CRU) gridded monthly data set (see http://www.cru.uea.ac.uk/) was selected as the observation data set to validate the multimodel ensemble (MME) simulations (Harris et al., 2020). The CRU data set is derived from the interpolation of observations at meteorological stations with a spatial resolution of $0.5° \times 0.5°$ and covers the mainland of the global surface for more than 50 years (Harris et al., 2014; Zhu et al., 2019). To examine the ability of MME in capturing the daily and seasonal precipitation patterns, a gridded daily observational data set, derived from the Asian Precipitation-Highly-Resolved Observational Data Integration Toward Evaluation (APHRODITE, hereafter APHRO) of the Water Resources project in Japan, was also used in this study (see http://aphrodite.st.hirosaki-u.ac.jp/). The APHRO data set was derived based on station observations with spatial resolutions of 0.25° (only for Japan) and of 0.5° covering the period from 1951 to the present day (Yatagai et al., 2012). In this study, the gridded daily precipitation data set was obtained with a spatial resolution of 0.5° from 1975 to 2004 for the purpose of model validation. Moreover, the APHRO data set and the MME simulation were regridded to match the CRU data set using the bilinear interpolation, in order to facilitate a quantitative comparison among the CRU data set, the APHRO product, and the MME simulation.

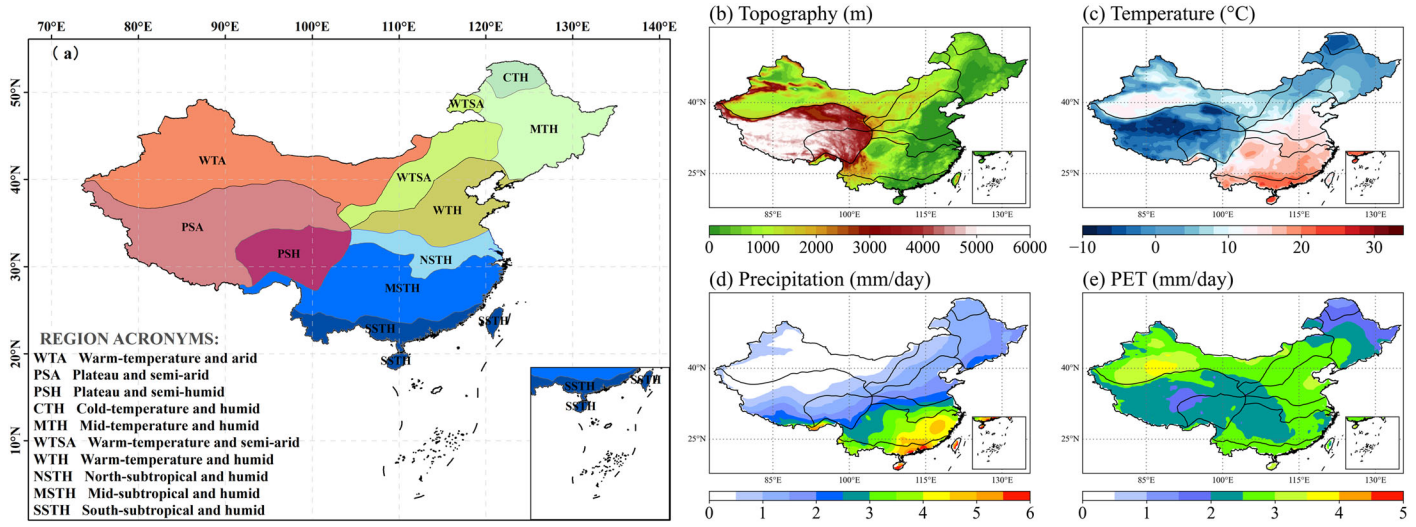

Figure 1. (a) Spatial distribution of the 10 major climate divisions covering China's land area, including West China (WTA, PSA, and PSH), Northeast China (CTH, MTH, WTSH, and WTH), and Southeast China (NSTH, MSTH, and SSTH); (b) Topography (m); The 30-year daily mean of (c) temperature, (d) precipitation, and (e) PET derived from the CRU data set.

Historical simulation and future projection of DWAA characteristics are analyzed using the MME mean values derived from five Coordinated Regional Climate Downscaling Experiment (CORDEX; see https://cordex.org/) East Asia experiments and the Providing Regional Climate Impacts for Studies (PRECIS) simulation for two 30-year periods, including a historical period of 1975–2004 and a future period of 2069–2098. The CORDEX data set with a spatial resolution of 0.44° was produced by dynamically downscaling four GCMs, including CNRM-CM5, EC-EARTH, MPI-ESM-LR, and HadGEM2 (Giorgi et al., 2012). The PRECIS model is an atmospheric and land surface model with a spatial resolution of 0.5° (Wilson et al., 2015), which shows good ability in climatological mean and extreme climate simulations over China (Zhu et al., 2019). A detailed description of experiments and climate models is provided in Table 1. To assess the DWAA characteristics, the MME simulation provides the important climate variables including precipitation and PET. In this study, PET was calculated using the FAO Penman-Monteith method based on air temperature, solar radiation, relative humidity, and wind speed obtained from the MME simulation (Zotarelli & Dukes, 2010). A detailed description about the PET method is included in Text S1 of the supporting information.

2.3. Extreme Indices

Precipitation and PET are dominant factors causing the water surplus or deficit. The potential interrelationships of DWAA and extreme precipitation events were explored in this study using the extreme precipitation indices including PR75p, PR85p, and PR95p. The tailed student *t* test was also used with the significance level of 0.05. PR75p, PR85p, and PR95p represent the gridded monthly cumulative number of days, with daily precipitation greater than the 75th percentile, the 85th percentile, and the 95th percentile of daily total

Table 1
List of Experiments and Climate Models Used in This Study

Experiment	Driving model	RCM	Variable	Spatial resolution	Temporal resolution
PRECIS	MOHC-HadGEM2-ES	PRECIS	P, T, R, H, W	0.5°	Mon; daily (P)
CORDEX	DMI-ICHEC	HIRHAM5	P, T, R, H, W	0.44°	Mon; daily (P)
CORDEX	MPI-ESM-LR	CCLM5-0-2	P, T, R, H, W	0.44°	Mon; daily (P)
CORDEX	EC-EARTH	CCLM5-0-2	P, T, R, H, W	0.44°	Mon; daily (P)
CORDEX	CNRM-CM5	CCLM5-0-2	P, T, R, H, W	0.44°	Mon; daily (P)
CORDEX	MOHC-HadGEM2-ES	CCLM5-0-2	P, T, R, H, W	0.44°	Mon; daily (P)

Note. RCM denotes the regional climate model. P, T, R, H, and W denote precipitation, temperature (mean, maximum, and minimum), solar radiation, relative humidity, and wind speed, respectively.

Table 2
SPEI Classification of Dry and Wet Conditions

SPEI value	Description
SPEI > = 2.0	Extreme wet
2.0 > SPEI > = 1.5	Severe wet
1.5 > SPEI > = 1.0	Moderate wet
1.0 > SPEI > − 1.0	Normal
−1.0 > = SPEI > − 1.5	Moderate dry
−1.5 > = SPEI > − 2.0	Severe dry
−2.0 > = SPEI	Extreme dry

precipitation, respectively. The precipitation percentile-based indices were used to define the intense and extreme rainfall events (Cao et al., 2018). The 75th percentile precipitation was also used in extreme precipitation studies at regional scales, such as in China (Cao et al., 2018) and the United States (Marquardt Collow et al., 2016). PR75p, PR85p, and PR95p on a monthly basis were thus used to define the frequency and magnitude of extreme precipitation for further investigation on the contribution of heavy rainfall with different intensities to DWAA over China.

In order to identify the onset and terminate of dry and wet spells for 10 climate divisions of China, the SPEI was calculated based on the difference between precipitation and PET to quantify water surplus and deficit (Vicente-Serrano et al., 2010). Although the SPEI was originally proposed for drought monitoring, it can also be used as a tool to detect flood risk (Xu et al., 2020). The SPEI is typically calculated by summing up the difference between precipitation and PET for 1 month and then by fitting the difference to a parametric probability distribution from which probability distributions are converted to the standard normal distribution (Beguería et al., 2014; McKee et al., 1993; Vicente-Serrano et al., 2010). The SPEI calculation method is introduced in Text S2 of the supporting information. According to the categories of SPEI, the climatic water condition can be divided into seven grades, as shown in Table 2. In this study, the gridded monthly SPEI was calculated based on the regridded monthly precipitation and PET derived from the MME simulations for the historical period of 1975–2004 and the future period of 2069–2098.

2.4. Identification of DWAA

Dry and wet spells can be represented by the SPEI values estimated to quantify the climatic water deficit and surplus conditions. In this study, the severe dry spell is defined by the SPEI value less than or equal to −1.5, while the severe wet spell is represented by the SPEI value greater than or equal to 1.5 (McKee et al., 1993). The threshold of 1.5 has been widely used in previous studies of climate extremes (Schaub & Finger, 2020; Vido et al., 2019; Yu et al., 2014). In addition, a sensitivity assessment on the thresholds of SPEI used to detect dry-wet transitions is depicted in section 3.3. The abrupt alternation between severe dry and severe wet spells in adjacent months is defined as the DWAA event using the 1-month SPEI. There are two types of DWAA events examined in this study. When a severe wet spell (SPEI > = 1.5) abruptly turns into a severe dry spell (SPEI <= − 1.5) due to the precipitation deficit or the intensified PET, this phenomenon is a wet-dry (W-D) alternation event. By contrast, when a severe dry spell (SPEI <= − 1.5) is suddenly terminated by a severe wet spell (SPEI > = 1.5) as a result of the increased precipitation, this phenomenon is a dry-wet (D-W) alternation event. Consequently, the potential links between two types of DWAA (W-D and D-W alternation events) and precipitation extremes with different intensities (PR75p, PR85p, and PR95p) as well as PET will be thoroughly examined to advance our understanding of the complex evolution of compound extremes.

3. Results and Discussion

3.1. Validation of MME Climate Simulations

As SPEI is estimated based on the difference between precipitation and PET, it is necessary to examine the ability of the MME simulation in reproducing precipitation and PET. Figure 2 shows the spatial distributions of 30-year mean temperature and precipitation over China, derived from the APHRO data set, the MME simulation, and the CRU observation for the period from 1975 to 2004. The APHRO shows that the multiyear mean temperatures are relatively low over Southwest China and Northeast China, and temperatures increase southward with a maximum detected in South China (Figure 2a). The mean temperatures generated from MME (Figure 2b) and CRU (Figure 2c) also exhibit similar spatial patterns. But the average precipitation amounts obtained from APHRO (Figure 2a) are relatively low over Northwest China and increase southeastward. The spatial distribution of average precipitation amounts from CRU is similar to those from APHRO. Comparing to APHRO and CRU, however, the MME-simulated average precipitation amounts are overestimated over South China. In fact, the overestimation of precipitation is found in many climate model simulations with relatively coarse resolution. It should be noted that the MME simulation is capable of reproducing a spatial pattern of mean temperature and precipitation over China even though the simulated

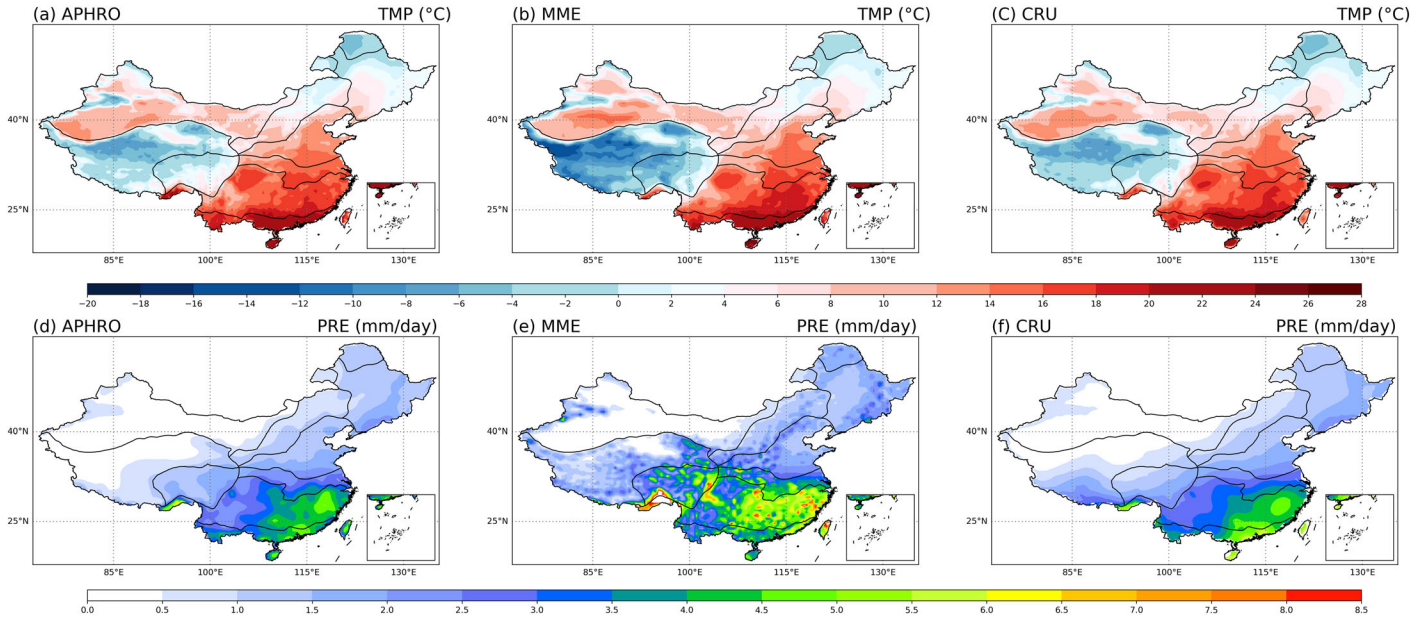

Figure 2. Spatial distribution of (top, a–c) average daily temperature and (bottom, d–f) average daily precipitation over China from 1975 to 2004 derived from (a, d) the APHRO product, (b, e) the MME simulation, and (c, f) the CRU observation, respectively.

precipitation is slightly overestimated over South China. Based on the MME simulation, the changes in SPEI and precipitation can then be calculated to generate the spatial distribution of DWAA events over China.

Figures 3a and 3b shows the spatial distribution of daily mean PET (mm) over China, derived from the MME simulation and the CRU observation for the period from 1975 to 2004. There is a similar spatial pattern of daily mean PET from MME and CRU. Figure 3c depicts the comparison of spatial patterns of daily PET differences between the MME mean and the CRU observation. It can be seen that PET is relatively high in Northwest and South China and relatively low in West China. These indicate the high skill of the MME simulation in performing a reliable assessment of DWAA events in comparison with the CRU observation over China.

As depicted in Figure 4, the precipitation extreme indices (PR75p, PR85p, and PR95p) derived from the MME simulation are validated against those derived from the APHRO product for the baseline period. PR75p represents the number of days in each month, with daily precipitation greater than the 75th percentile of daily total precipitation for the baseline period. It can be seen that the spatial patterns of PR75p (Figures 4a–4c) and PR85p (Figures 4d–4f) are well simulated by the MME. Both low precipitation extremes in the arid regions of Northwest China and high precipitation extremes in the wet regions of Northeast and Southeast China are well captured. However, the MME simulation tends to underestimate the low values

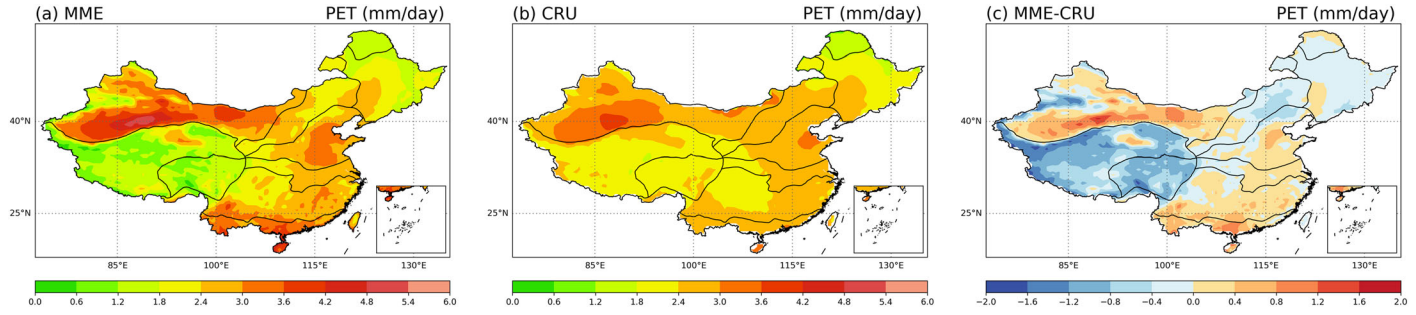

Figure 3. Spatial distribution of average daily PET over China from 1975 to 2004 derived from (a) the MME simulation, (b) the CRU observation, and (c) the difference between MME and CRU.

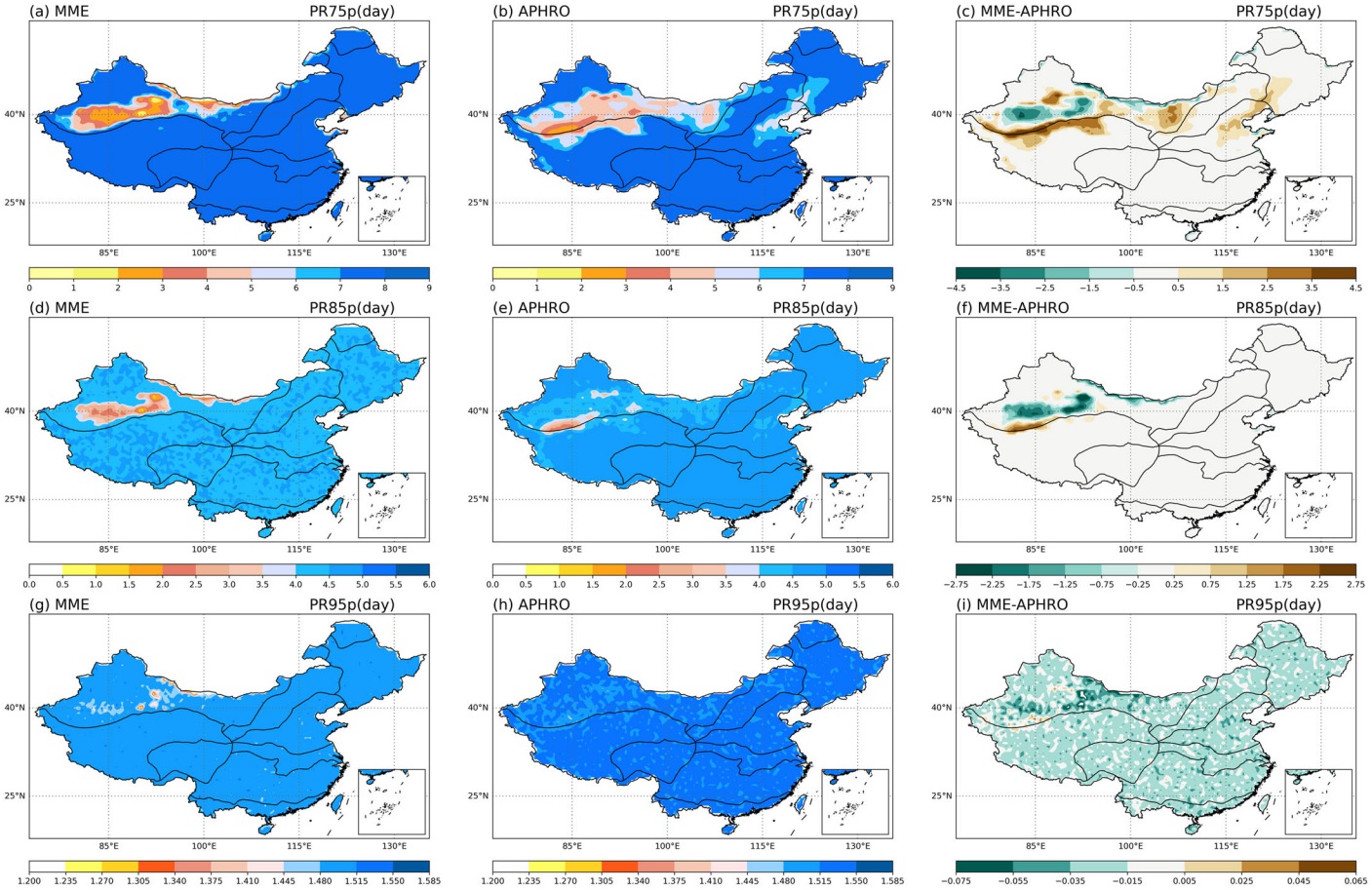

Figure 4. Spatial distribution of (top, a–c) PR75p, (middle, d–f) PR85p, and (bottom, g–i) PR95p over China from 1975 to 2004, derived from (first column, a, d, g) the MME simulation, (second column, b, e, h) the APHRO product, and (third column, c, f, i) the difference between MME and APHRO.

over the middle part of Northwest China and overestimate them in the lower part of Northwest China. PR95p (Figures 4g–4i) represents the number of days in each month, with daily precipitation greater than the 95th percentile of daily total precipitation for the baseline period. The MME simulation shows a similar spatial distribution with APHRO, with a slight overestimation over Northwest China. Therefore, the MME can be used to simulate the spatial distribution of precipitation extremes over China. In light of the agreement between the MME simulations and the observation data sets (the APHRO product and the CRU data set), the MME is capable of simulating climatic features (precipitation, temperature, and PET) over China and can thus be used to identify the hot spots of DWAA events.

3.2. Projected Changes in Precipitation Extremes and PET

To investigate the possible cause of the observed intensification of extreme events, the seasonal changes in precipitation and PET are analyzed for historical and future periods. Figure 5 represents the averages of PR95p derived from the MME simulation against those derived from the APHRO product for 10 climate divisions of China during 1975–2004. It can be seen that the peak number of heavy rainfall events often appears in summer (June, July, and August) for most climate divisions, whereas the largest number of heavy rainfall events detected in April rather than summer over the north-subtropical and humid (NSTH) region. Moreover, the precipitation patterns, in terms of the number of heavy rainfall events, are relatively underestimated in the warm temperature and arid (WTA) region. Overall, our findings reveal the prominent seasonal precipitation characteristics with more heavy rainfall events occurring in summer and less in winter over China. The averages of PR75p and PR85p derived from the MME simulation against those derived from the APHRO product are also depicted in Figures S1 and S2 of the supporting information.

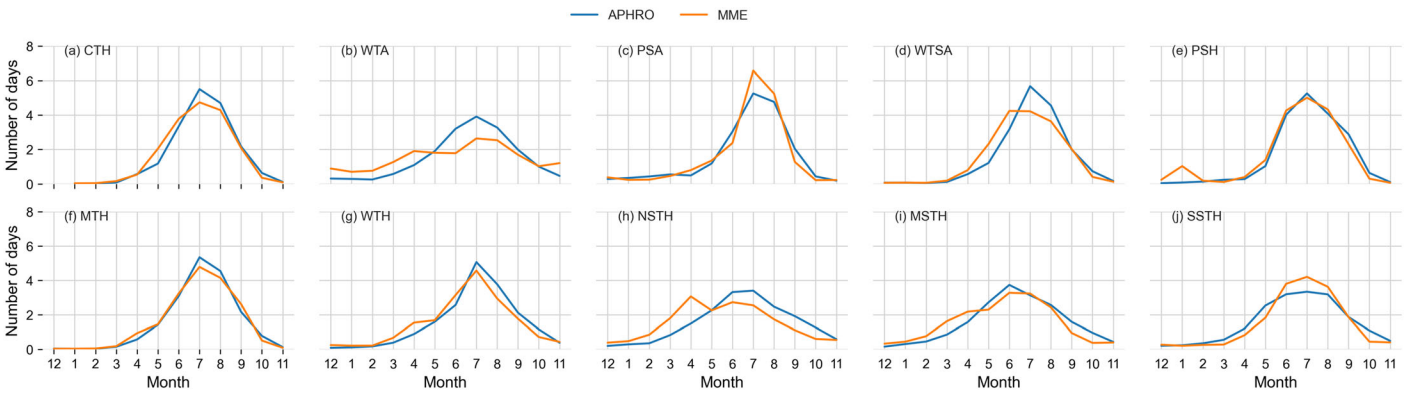

Figure 5. (a–j) The annual cycle of PR95p over 10 climate divisions of China, derived from the MME simulation (orange lines) and the APHRO product (blue lines).

Figure S3 shows the projected changes in the PR75p, PR85p, and PR95p for the period of 2069–2098 relative to the baseline period. The MME simulation shows a general increase in the number of heavy rainfall events over West and Northeast China, with relatively few events occurring in Southeast China, especially in the Yunnan-Kweichow Plateau (located in between 22°N and 30°N, 100°E and 111°E). To further understand the changes in the occurrence of heavy rainfall events, Figure 6 shows the future changes in the PR95p over 10 climate divisions of China for the rainy seasons including spring (March, April, May) and summer (June, July, and August). The PR95p is projected to increase for most parts of China by the end of this century, except for the southernmost region (SSTH) that shows a decreasing trend in March, April, July, and August as well as for North Central China (WTSA) with a decreasing trend in June. Moreover, there is a considerable spatial variation in the PR95p in July. Specifically, there is an increasing trend in West China (PSA and PSH) and Central China (WTSA, NSTH, and MSTH), whereas the PR95p is expected to decrease slightly in several northernmost regions (WTA, CTH, MTH, and WTH) and the southernmost region (SSTH).

Figure 7 presents the projected changes in annual and seasonal mean PET for the future period of 2069–2098 relative to the baseline period. There is a prominent increase in PET over Northwest and South China, and a decreasing tendency is projected to appear over Northeast and Southwest China. Similar patterns are detected for the changes of PET across different seasons. Specifically, a decreasing tendency is expected to appear in winter and spring over Southwest China. And the largest increase of PET is expected to appear in summer, especially for Northwest and South China. This could be caused by a downward trend of relative humidity and an upward trend of air temperature (Zhao et al., 2020).

3.3. Temporal and Spatial Evolution of DWAA Events

To facilitate an in-depth understanding of DWAA events in China, a sensitivity assessment on the thresholds of SPEI used to detect DWAA was also carried out in this study. Previous studies identified the drought by the threshold of smaller than −0.8 (Qing et al., 2020) or −1.0 (Su et al., 2018), which could lead to a large number of the swings between dry and wet spells. However, the threshold of smaller than −0.8 or −1 did not indicate a severe drought. Instead, the threshold of smaller than −1.5 (or larger than 1.5) can be used to represent a severe dry spell (or a severe wet spell). Figure S4 represents the spatial distribution of the annual average number of DWAA events identified using three different thresholds (±0.8, ±1.0, and ±1.5) for the historical period of 1975–2004. The decreasing number of detected DWAA events is mainly due to the selection of the relatively large threshold of ±1.5 (SPEI <= − 1.5 indicates a dry condition and SPEI > = 1.5 indicates a wet condition). The transition between dry and wet spells appears over Northeast and Central East China, particularly for NSTH. Since the spatial distribution detected by the threshold of ±1.5 exhibits a more prominent spatial heterogeneity in comparison with other thresholds, the threshold of ±1.5 was used to detect the DWAA event over China. In general, the detection of DWAA events provides meaningful insights into the geographical hot spots of severe compound extreme events (i.e. the abrupt transition between dry and wet extremes), which plays a crucial role in helping policymakers and stakeholders develop adaptation plans for reducing potential damages caused by compound effects of climate events.

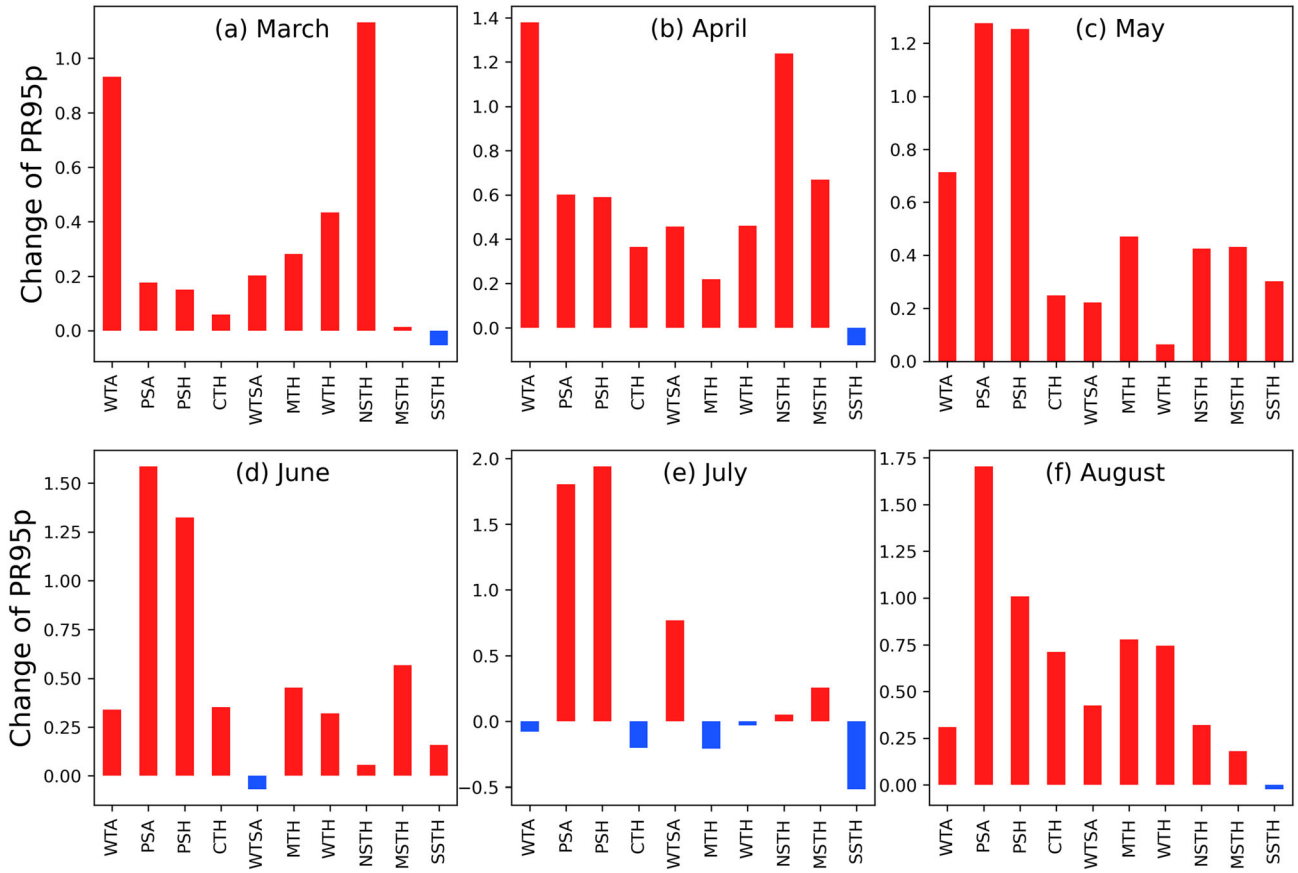

Figure 6. Projected changes in the area-averaged PR95p in spring (March, April, and May) and summer (June, July, and August) across 10 climate divisions of China for 2069–2098 relative to 1975–2004. The red and blue bars represent the increasing and decreasing PR95p, respectively.

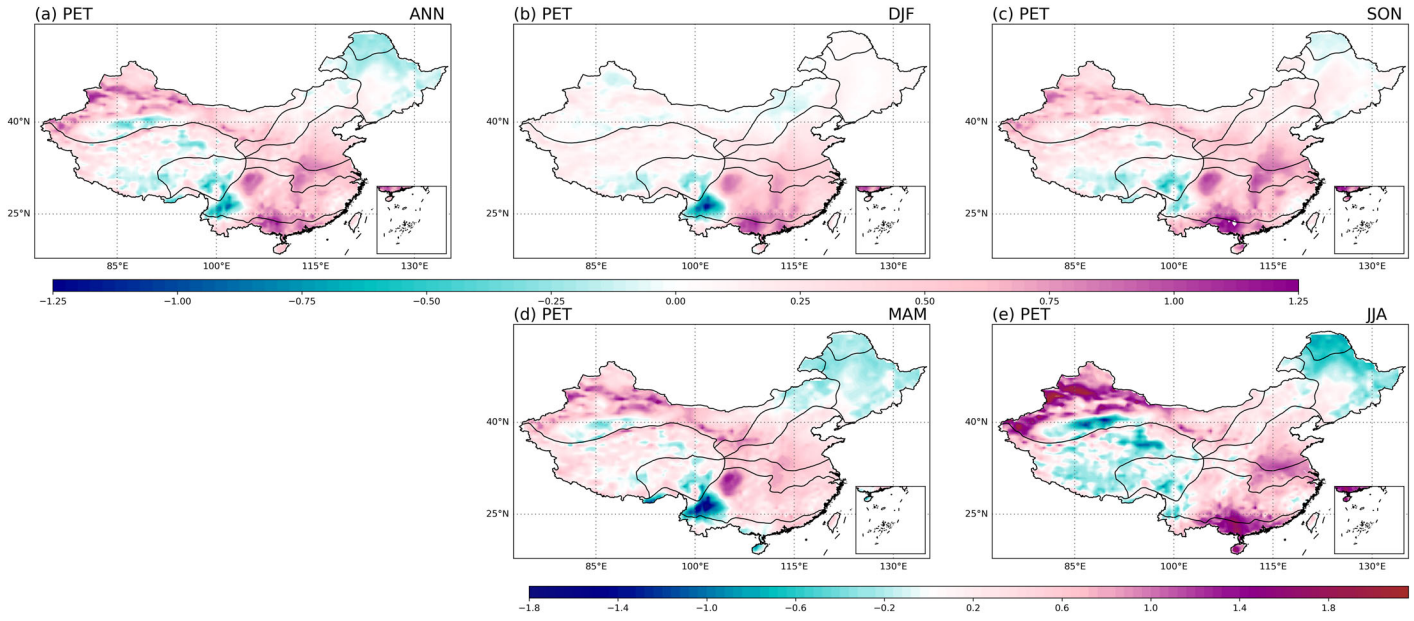

Figure 7. Spatial distribution of projected changes in the 30-year average daily PET over China for (a) annual (Ann), (b) winter (DJF), (c) fall (SON), (d) spring (MAM), and (e) summer (JJA).

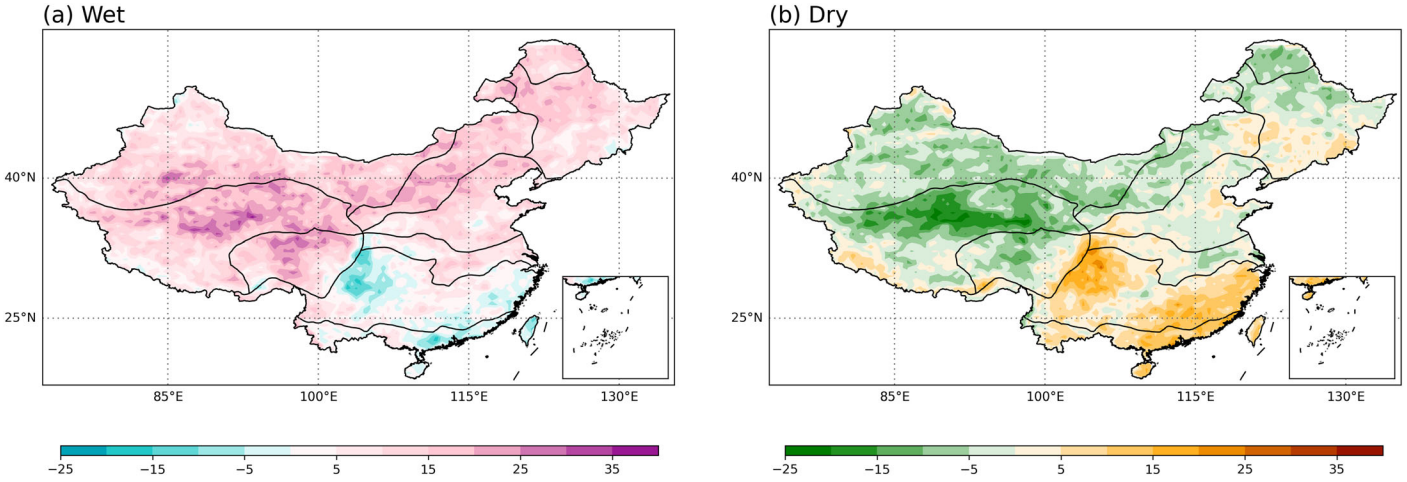

Figure 8. Spatial distribution of projected changes in the 30-year total number of (a) severe wet months and (b) severe dry months for the future period of 2069–2098 relative to the historical period of 1975–2004.

To examine the relative changes in wet and dry periods, the total number of wet and dry months is compared between the future period of 2069–2098 and the historical period of 1975–2004 at each grid cell without considering the extent of extreme events. By using the SPEI, the projected changes in the total number of wet and dry months are shown in Figure 8. The wet months are projected to appear more frequently in the West and Northeast China (Figure 8a), with less frequent dry months (Figure 8b). By contrast, the less frequent wet months (Figure 8a) and the more frequent dry months (Figure 8b) are expected to appear in Southeast China. These results are in agreement with previous studies that West China will become wetter and South China will become drier under climate change (Zhang et al., 2012).

Figure 9 shows the projected seasonal changes in the total number of wet and dry months. The frequency of wet spells shows an obvious upward trend in West and Northeast China and a downward trend in Southeast China for winter and fall, but an opposite trend is observed for the frequency of dry spells. Moreover, the frequency of wet spells increases in spring for most parts of North China. Meanwhile, the

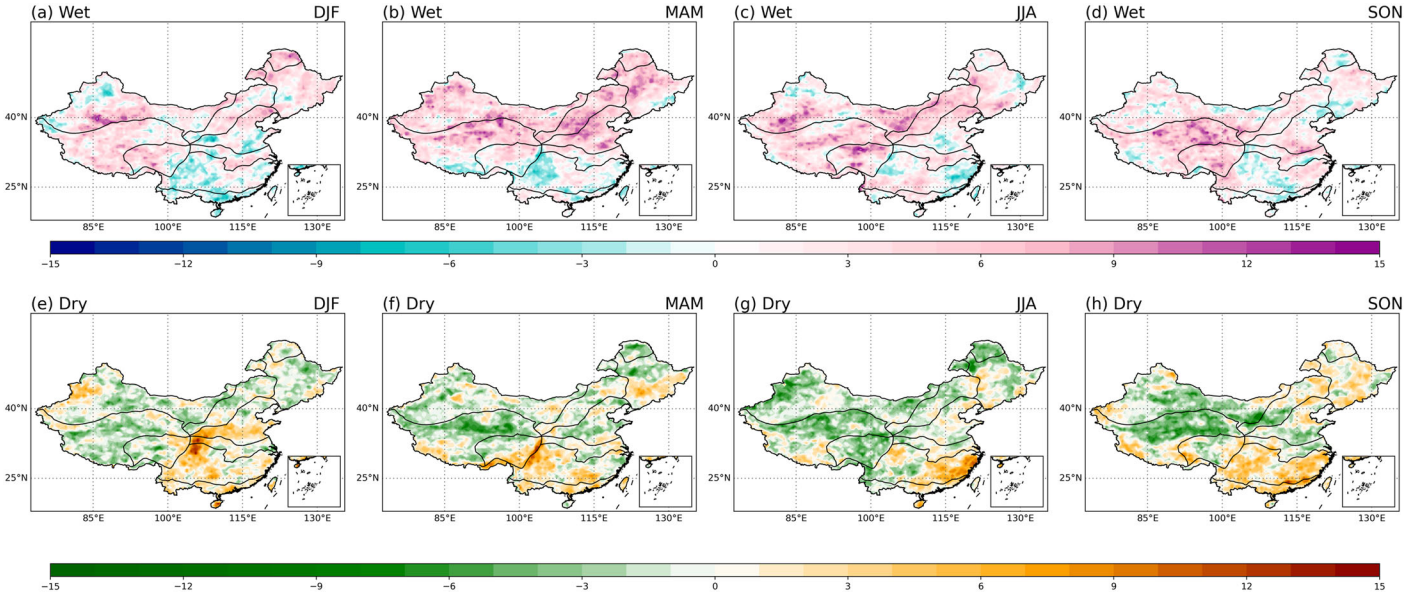

Figure 9. Spatial distribution of projected changes in the 30-year total number of (top, a–d) seasonal severe wet months and (bottom, e–h) seasonal dry months for the future period of 2069–2098 relative to the historical period of 1975–004.

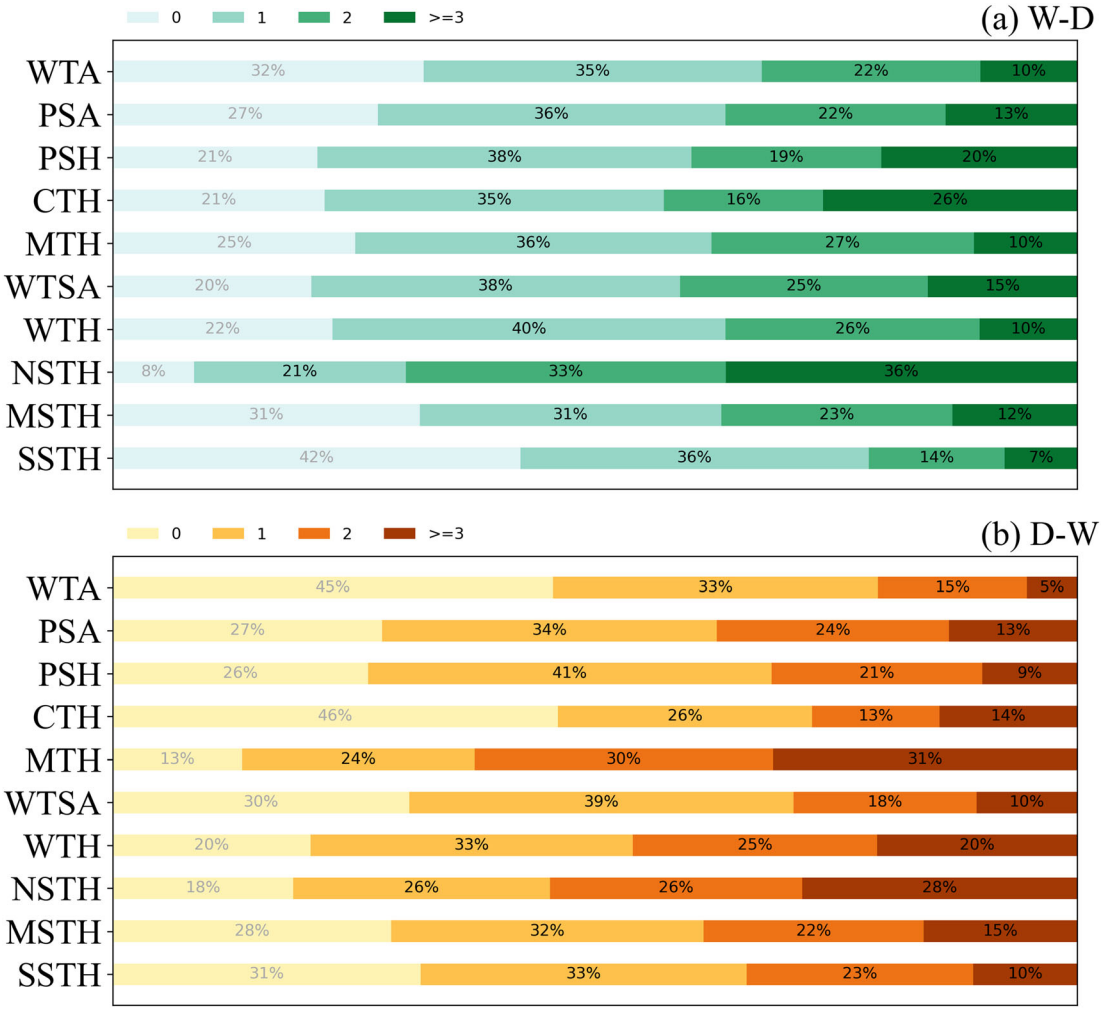

Figure 10. The percentage frequency of occurrence of gridded (a) W-D alternation events and (b) D-W alternation events based on different categories (none, 1, 2, and greater than or equal to 3) across 10 climate divisions of China during the historical period of 1975–2004.

frequency of dry spells decreases in Northwest, Northernmost and Central East China, excluding Southeast China that shows an increasing frequency of dry spells. The positive trend in the frequency of wet spells is prominent for the summer season over Southwest and North China; meanwhile, a negative trend in the frequency of dry spells is observed in Southwest China.

The wet-dry (W-D) alternation event is characterized by a wet condition occurring in the *i*th month and abruptly turning into a dry condition in the i + 1st month. The percentage frequency of occurrence of gridded W-D alternation events is estimated based on different categories, including none, 1, 2, and greater than or equal to 3, for 10 climate divisions of China during the period of 1975–2004, as shown in Figure 10a. The color bar represents the percentage of grid cells (i.e. land area) within a specific category (none, 1, 2, and greater than or equal to 3) for the frequency of W-D alternation events detected in each of the 10 climate divisions of China. In general, a total of 73% of China's land area suffered from the W-D alternation event at least once during 1975–2004, including 35% of the land area occurring once, 24% of the land area occurring twice, and 14% of the land area occurring greater than or equal to three times. However, it can be seen that NSTH has the largest percentage of the land area occurring the W-D alternation event, with 92% of the land area occurring more than once and 36% of the land area occurring greater than or equal to three times.

Figure 10b shows that the percentage frequency of occurrence of gridded dry-wet (D-W) alternation events for 10 climate divisions of China. The D-W alternation event occurred at least once for a total of 70% of the land area in China, including 33% for once, 22% for twice, and 15% for greater than or equal to three times.

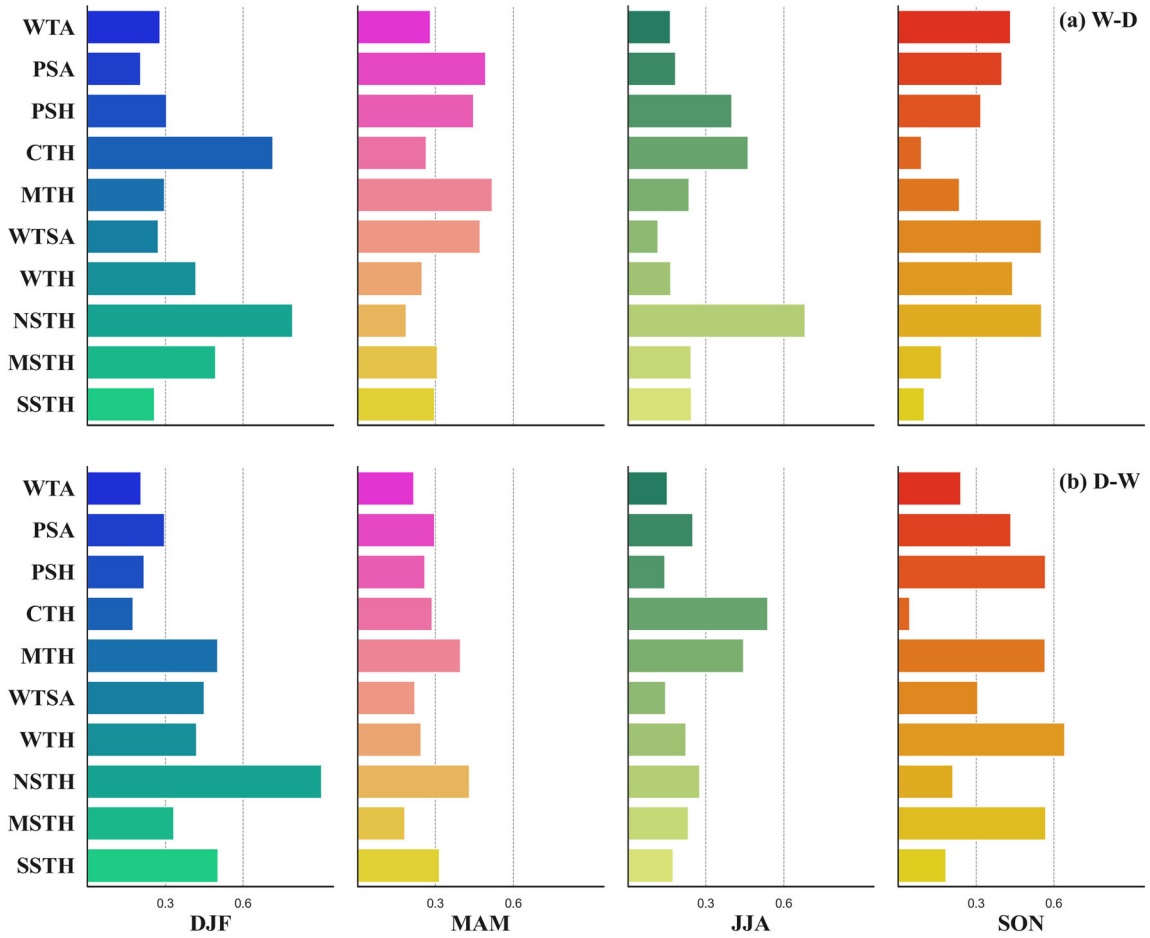

Figure 11. The area-weighted average of the total number of (a) W-D alternation events and (b) D-W alternation events across different seasons for 10 climate divisions of China during the historical period of 1975–2004.

Similar to the occurrence of W-D alternation events, the detected area is decreasing for most climate divisions of China (except for CTH, MTH, and NSTH) when the number of D-W alteration events is increasing. Moreover, MTH is the most severe climate division suffering from the D-W alternation event, with 87% of the land area occurring at least once and 31% of the land area occurring greater than or equal to three times. NSTH is the second severe climate division suffering from the D-W alternation event, with 82% of the land area occurring at least once and 28% of the land area occurring greater than or equal to three times.

Figure 11a shows that the area-averaged number of W-D alternation events detected across different seasons during the period of 1975–2004. It can be seen that the northernmost part of China (CTH) and Central China (WTH, NSTH, and MSTH) experienced a relatively large number of W-D alternation events in winter (DJF), and the regions of West China (PSA and PSH) and Northeast China (MTH and WTSA) suffered from a relatively frequent occurrence of W-D alternation events in spring (MAM). In summer (JJA), a relatively large number of W-D alternation events occurred over the northernmost part of China (CTH) and Central China (PSH and NSTH), and the W-D alternation events occurred more frequently in fall (SON) over West China (WTA, PSA, and PSH) and Central South China (WTSA, WTH, and NSTH).

Figure 11b shows that the area-averaged number of D-W alternation events occurred across different seasons over China. It is indicated that the D-W alternation events occurred relatively frequently in winter for most parts of East China (except for CTH). For the warm seasons (spring and summer), there is a relatively low frequency of occurrence of D-W alternation events for almost all climate divisions, except for CTH and MTH in Northeast China. In comparison, there is a more frequent occurrence of D-W alternation events in fall, especially in West China (PSA and PSH) and Central China (MTH, WTH, and MSTH). Overall, the wintertime DWAA events, including W-D and D-W alternation events, occurred relatively frequently in

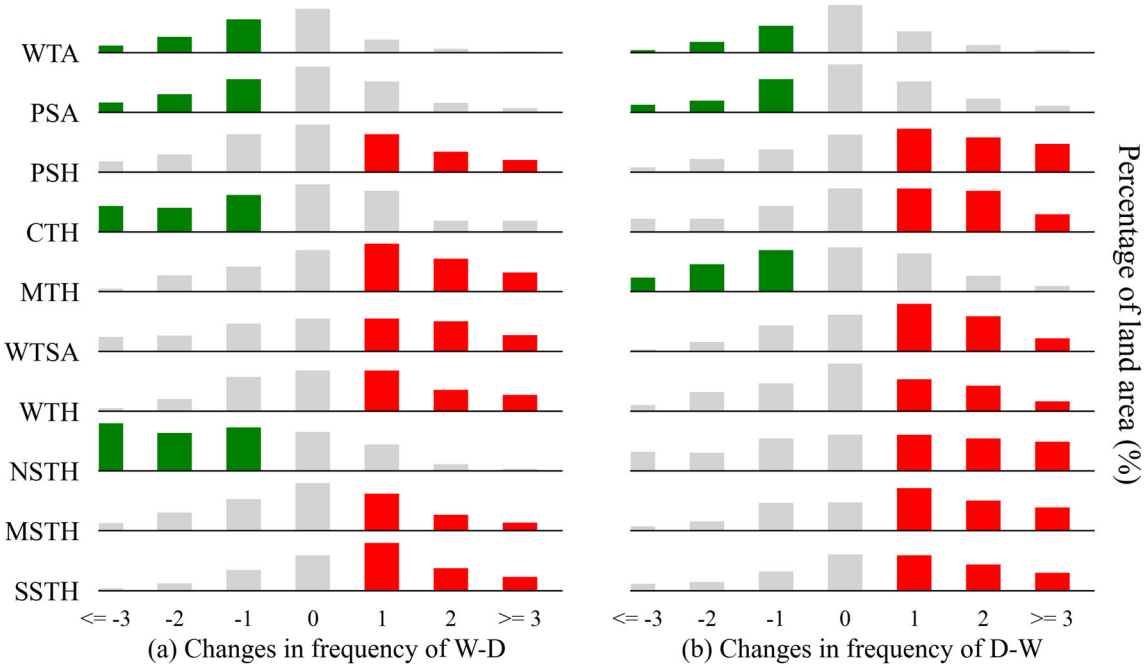

Figure 12. Projected changes in the percentage frequency of gridded (a) W-D alternation and (b) D-W alternation events between the future period of 2069–2098 and the historical period of 1975–2004 for 10 climate divisions of China. The value equal to 0 represents no difference in the occurrence of DWAA events; the value greater than 0 represents a more frequent occurrence of DWAA events, and the value smaller than 0 represents the less frequent occurrence of DWAA events. The red bar represents the more frequent occurrence of DWAA events. The green bar represents the land area experiencing the less frequent occurrence of DWAA events.

South China, while there was a relatively large number of DWAA events detected in fall for most parts of China, except for SSTH and CTH.

As for the future changes in spatial features of DWAA events (Figure 12), the less frequent DWAA events are expected to be more widespread in West China (WTA and PSA), while the more frequent DWAA events are projected to be more predominant in Central North China (PSH, WTSA, and WTH) and Southeast China (MSTH and SSTH). Specifically, the increased W-D alternation events are projected to be more dominant while the decreased D-W alternation events are expected to be more prominent in Northeast China (MTH). The opposite pattern is observed in CTH and NSTH, where the decreased W-D alternation events are projected to be more widespread while the increased D-W alternation events are expected to be more prominent.

Figure 13 shows the future changes in the area-averaged frequency of DWAA events across different seasons over 10 climate divisions. As for the occurrence of W-D alternation events (Figure 13a), an increasing tendency is projected in summer for most climate divisions, except for WTA, CTH, and NSTH that show a decreasing tendency. A similar tendency is expected in winter, with most climate divisions showing an upward tendency except for WTA, CTH, NSTH, and MSTH showing a downward tendency. A decreasing tendency is expected in spring for most parts of China, excluding WTH and NSTH. In fall, a decreasing tendency is projected for five of China's climate divisions (WTA, PSA, CTH, WTSA, and NSTH), while an increasing tendency is expected for the other climate divisions. As for the occurrence of D-W alternation events (Figure 13b), an upward tendency is projected in summer for about half of China's land area, excluding WTA, CTH, MTH, and NSTH which are projected to have a downward tendency. An increasing frequency of D-W alternation events is projected in spring over East China, while a slightly decreasing tendency is projected in Northwest China (WTA and PSA). Moreover, there is a slightly increasing tendency of D-W alternation events in winter for most land areas of China, while a decreasing tendency is expected in WTA, MTH, and NSTH. In fall, there is also an increasing tendency of D-W alternation events for most parts of China, except for PSA, WTH, and MSTH. In general, the frequency of W-D alternation events is projected to greatly increase in summer, and a prominent increase of D-W alternation events is expected in spring for

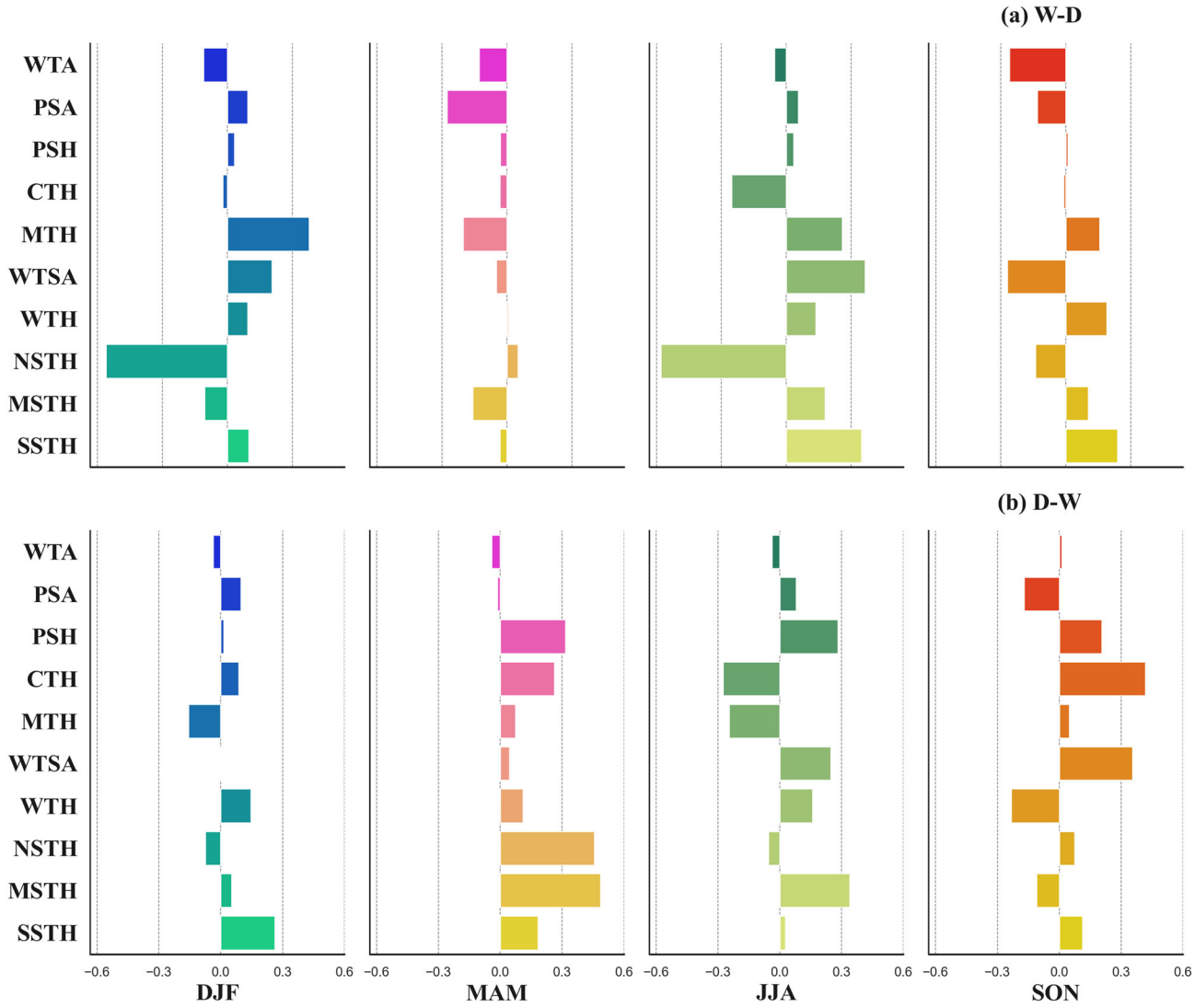

Figure 13. Projected changes in the area-weighted average of the number of (a) W-D alternation events and (b) D-W alternation events across different seasons for 10 climate divisions of China. The value greater than 0 represents that the DWAA event is projected to become more frequent, while the value smaller than 0 indicates that the DWAA event is expected to become less frequent.

most parts of East China. As a result, the rapid transitions between dry and wet spells in warm seasons will pose a severe threat to agriculture development and food production, which should receive serious attention to reduce potential damages caused by the emerging extreme events.

Figure 14 depicts the changes in the magnitude of W-D and D-W alternation events for the future period of 2069–2098 relative to the baseline period of 1975–2004. The magnitude is defined as the difference of SPEI values derived from two adjacent months in a DWAA event (magnitude = $SPEI_i - SPEI_{i+1}$, when $SPEI_i >= 1.5$ or $SPEI_i <= -1.5$), which can be used to quantify the intensity of the DWAA event. As shown in Figure 14a, the W-D alternation event is projected to become more intense with a larger magnitude for most parts of China, excluding the northernmost part of China (CTH) and Central China (PSH and MSTH). By contrast, the regions of East Central China are expected to experience an increasing magnitude of D-W alternation events (Figure 14b), including MTH and WTH. In general, more frequent occurrence of the W-D alternation event with a larger magnitude is expected to appear in MTH, WTSA, WTH, and SSTH. The more frequent occurrence of the W-D alternation event with a smaller magnitude is projected to appear for only a few regions (PSH and MSTH). Moreover, less frequent occurrence of the W-D alternation event with a larger magnitude is projected to appear in WTA, PSA, and NSTH. In

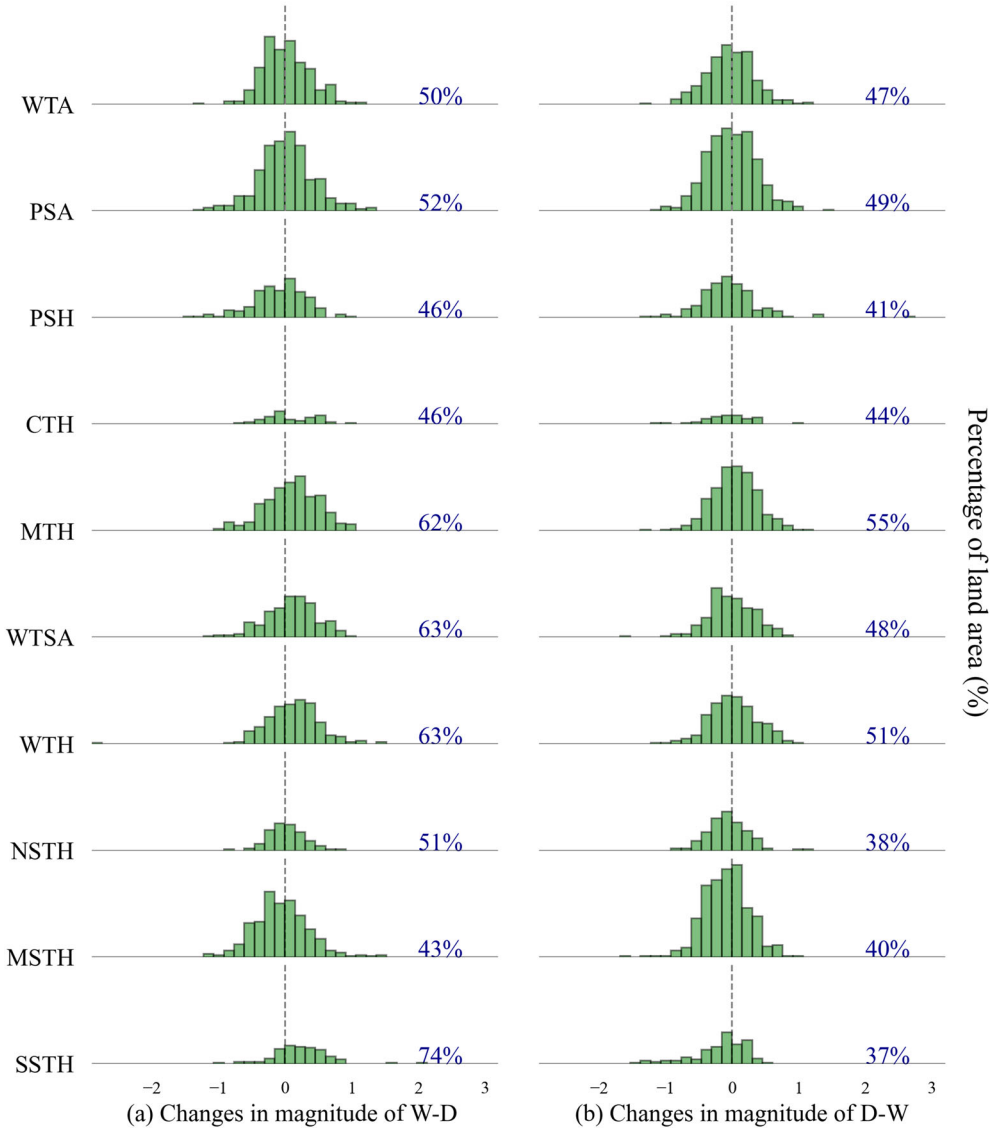

Figure 14. Projected changes in the magnitude of (a) W-D alternation events and (b) D-W alternation events for 10 climate divisions of China. The magnitude is defined as the difference of the SPEI values calculated in adjacent months when a DWAA event occurs. The right-hand side of the dashed line represents that the DWAA events are projected to become more intense with a larger magnitude for the future period of 2069–2098, and the value represents the percentage of land area detected in the right-hand side of the dashed line.

addition, the D-W alternation event is projected to become more frequent with a smaller magnitude for six climate divisions of China, including PSH, CTH, WTSA, NSTH, MSTH, and SSTH. The more frequent occurrence of the D-W alternation event with a larger magnitude is projected to appear in WTH. It should be noted that the region with both an intensified magnitude and an increased frequency of DWAA events is projected to appear in the North China Plain, where it is dominated by the warm temperature and humid (WTH) climate and more than half of the land area (63% for the occurrence of W-D alternation events and 51% for the occurrence of D-W alternation events) is expected to suffer from the more intense DWAA events with an increasing magnitude. The DWAA event is projected to be arguably more hazardous in the North China Plain which is one of the most densely populated region and is also the most important growing region in China, and thus, urgent actions are needed to mitigate climate change impacts on the emerging compound extremes.

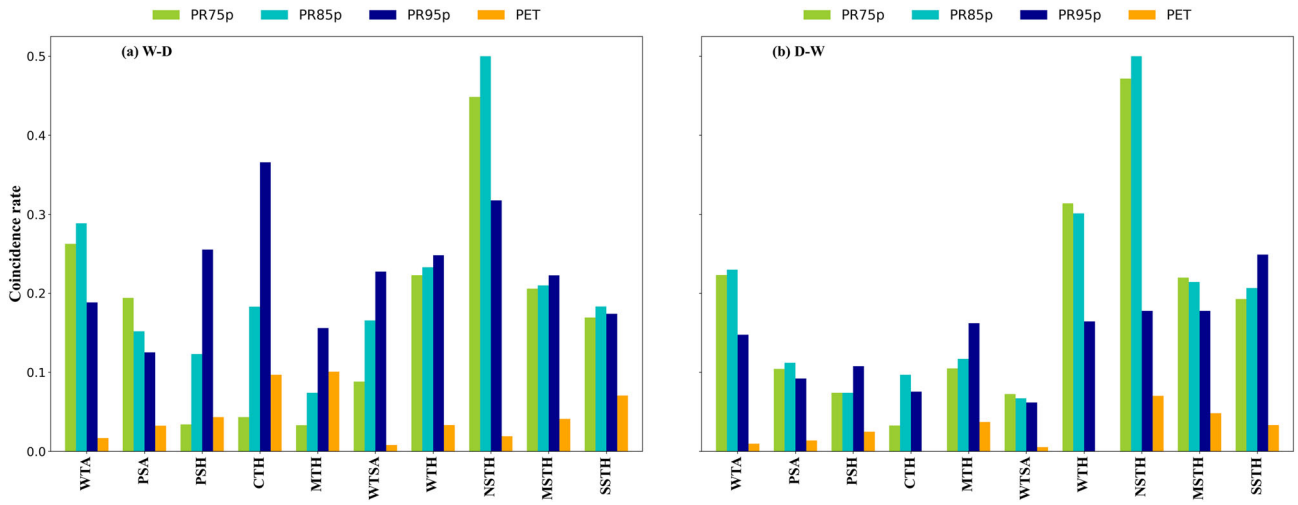

Figure 15. (a, b) The rates of coincidence between DWAA events and heavy rainfall with different intensities (PR75p, PR85p, and PR95p) for 10 climate divisions of China in the historical period of 1975–2004. The coincidence rate is defined as the coefficient of a strong correlation ($R >= 0.8$) between DWAA events and heavy rainfall at the significance level of 5%.

3.4. Interrelationships of DWAA, Heavy Rainfall, and PET

To further explore the dominant factors (rainfall and PET) contributing to the occurrence of DWAA events, the Pearson's correlation coefficient (R value) and t test (p value) were used to assess the interrelationships between the gridded DWAA events and heavy rainfall with different intensities (PR75p, PR85p, and PR95p) as well as PET for the 2 months before and after the occurrence of each DWAA event. Figure 15 presents the area-averaged rate of coincidence between DWAA events and heavy rainfall as well as PET for 10 climate divisions of China in the historical period of 1975–2004. The coincidence rate is defined as the strong correlation coefficient ($R >=0.8$ for heavy rainfall and $R <= -0.8$ for PET) for the concurrence of DWAA and

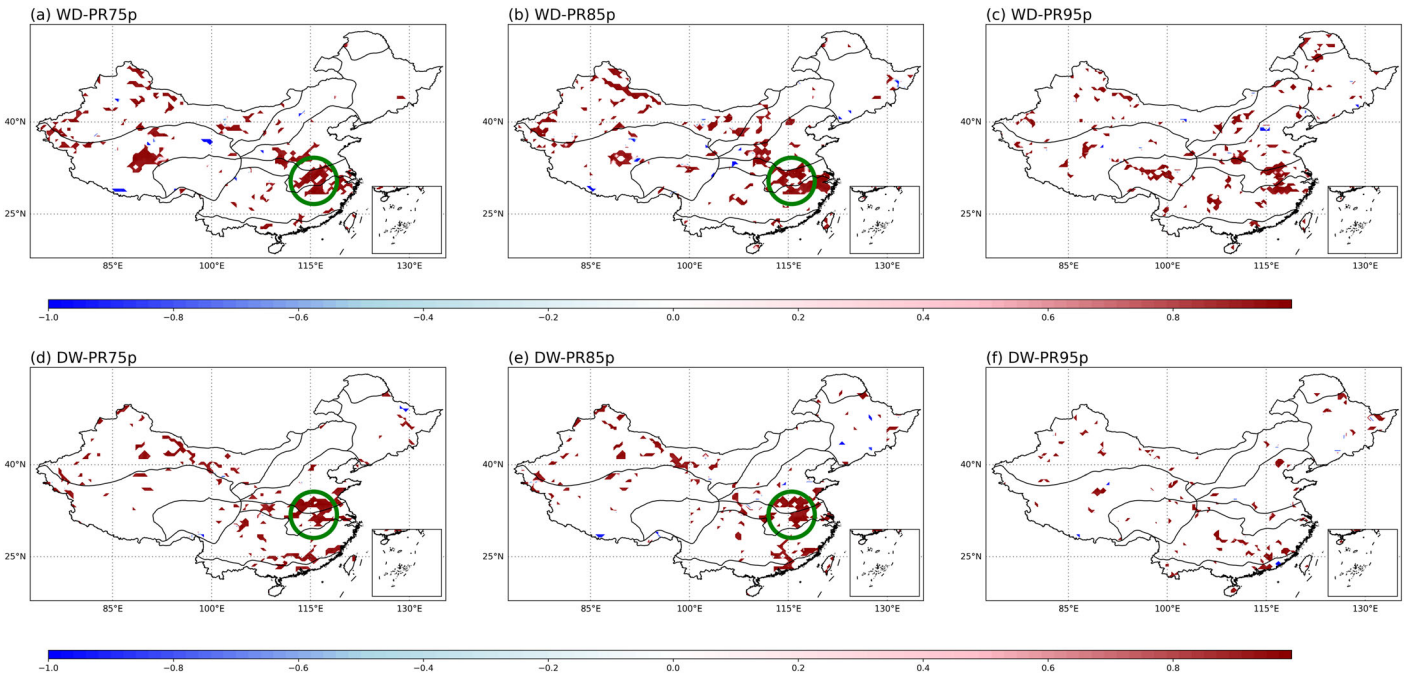

Figure 16. (a–f) Spatial distribution of interrelationships between DWAA events and heavy rainfall with different intensities (PR75p, PR85p, and PR95p). The climate division of NSTH is highlighted by green circle.

heavy rainfall events as well as monthly PET at the significance level of 5%. It can be seen that the majority of China's land area has the coincidence rates between 10% and 30% for the concurrence of DWAA and heavy rainfall events, while China's land area has the coincidence rates less than 10% for the concurrence of DWAA and monthly PET variability. And NSTH has the coincidence rate exceeding 40%, indicating that there is a strong relationship between the occurrence of DWAA and the 75th and 85th percentile rainfall events. For the regions of West China (WTA and PSA) and NSTH, there is a relatively high rate of coincidence between DWAA and the 75th and 85th percentile rainfall events. In fact, the majority of China's land area experienced a relatively high rate of coincidence between the occurrence of the W-D alternation and the 95th percentile rainfall events, including PSH, CTH, MTH, WTSA, WTH, and MSTH. By contrast, most regions of China had a higher rate of coincidence between the occurrence of the D-W alternation and the 75th and 85th percentile rainfall events, excluding PSH, MTH, and SSTH. In other words, the 95th percentile rainfall event contributes most to the occurrence of W-D alternation events over more than half of China's land area, while the 85th percentile rainfall events contribute more to the occurrence of D-W alternation events for more than half of China's land area.

Figure 16 shows the spatial distribution of mean correlation coefficients (R values at the significance level of 5%) derived for the concurrence of DWAA and heavy rainfall. There is a strong positive correlation between DWAA events and precipitation extremes at a significance level of 5%. The climate division of NSTH, highlighted by green circle in Figure 16, suffered badly from the concurrence of DWAA and the 75th and 85th percentile rainfall events. The NSTH is situated in a transitional climate zone under the influence of the humid subtropical climate in the south and the warm temperature semihumid climate in the north. The average annual precipitation in this division is approximately 900 mm. The precipitation exhibits a large temporal variability, with more than 60% of annual precipitation concentrated over a few months, especially for the Meiyu front in late spring and early summer. The Meiyu front generates a persistent stationary rain (PR75p and PR85p) in late spring, which ends the early spring drought (Feng et al., 2012; Wang et al., 2009). Compared with the 75th and 85th percentile rainfall events, we find less organized spatial structures for the 95th percentile rainfall events contributing to the occurrence of DWAA events.

4. Conclusions

This study explores future changes in the abrupt alternation between dry and wet extremes over China through an ensemble of regional climate model simulations including five CORDEX East Asia experiments and one PRECIS experiment. We attempt to explore the dynamic evolution of DWAA events including the geographical hot spots of DWAA events and to investigate whether DWAA is becoming more widespread under climate change. Moreover, we examine the interrelationships between two types of DWAA events (W-D and D-W alternation events) and precipitation extremes with different intensities as well as PET, which plays a crucial role in advancing our understanding of DWAA mechanisms and compound effects of hydrological extremes in a changing climate.

Our findings reveal that a total of 70% of China's land area suffered from the DWAA event at least once during 1975–2004. The climate division of NSTH is identified as the China's hot spot experiencing the most frequent occurrence of DWAA events with a relatively large affected area in the historical period. The DWAA events are projected to occur more frequently with a greater intensity in the North China Plain which is dominated by the WTH climate and has dense population and agriculture production activities. A substantial increase of the W-D alternation event is projected to appear in summer, while a prominent increase of the D-W alternation event is expected in spring for most parts of East China. In addition, a strong positive correlation between DWAA and heavy rainfall is detected. Specifically, the 95th percentile rainfall event contributes most to the occurrence of W-D alternation events, while the 85th percentile rainfall event has the most significant correlation with the D-W alternation event. For most climate divisions of China, we find that there will be an increase in either the frequency or the magnitude of DWAA events, thereby leading to great potential risks associated with the rapid transition between dry and wet extremes. Consequently, the projected changes of DWAA provide meaningful insights into the risk assessment of compound extremes, which facilitate policymakers and stakeholders to develop sound adaptation plans.

It should be noted that the MME climate simulations were conducted in this study under the highest emission scenario of RCP8.5. The projected changes of DWAA characteristics will vary under different future

emission scenarios. In addition, we focused on the rapid transition between dry and wet extremes in two adjacent months for each grid cell but did not consider the duration and extent of a dry or a wet spell. Future studies should be undertaken to take into account various characteristics of dry and wet extremes in order to further improve the assessment and projection of complex DWAA events.

Data Availability Statement

The precipitation and PET were derived from various sources, including the CRU data set, the APHRODITE product, five CORDEX experiments, and the PRECIS experiment that can be accessed online (https://data.mendeley.com/datasets/s6yj9t2rcy/2).

Acknowledgments

This research was supported by the National Natural Science Foundation of China (Grant 51809223) and the Hong Kong Research Grants Council Early Career Scheme (Grant PP5Z). We would like to express our sincere gratitude to the Editor and anonymous reviewers for their constructive comments and suggestions.

References

Annamalai, H., Global, U. K. U, & Modelling, A. (2001). Active/break cycles: Diagnosis of the intraseasonal variability of the Asian summer monsoon. *Climate Dynamics*, *18*, 85–102. https://doi.org/10.1007/s003820100161

Beguería, S., Vicente-Serrano, S. M., Reig, F., & Latorre, B. (2014). Standardized precipitation evapotranspiration index (SPEI) revisited: Parameter fitting, evapotranspiration models, tools, datasets and drought monitoring. *International Journal of Climatology*, *34*(10), 3001–3023. https://doi.org/10.1002/joc.3887

Cao, F., Gao, T., Dan, L., Ma, Z., Yang, X., & Yang, F. (2018). Contribution of large-scale circulation anomalies to variability of summer precipitation extremes in northeast China. *Atmospheric Science Letters*, *19*(12), 1–11. https://doi.org/10.1002/asl.867

Carvalho, K. S., & Wang, S. (2020). Sea surface temperature variability in the Arctic Ocean and its marginal seas in a changing climate: Patterns and mechanisms. *Global and Planetary Change*, *193*, 103265. https://doi.org/10.1016/j.gloplacha.2020.103265

Chen, H., Wang, S., & Wang, Y. (2020). Exploring abrupt alternations between wet and dry conditions on the basis of historical observations and convection-permitting climate model simulations. *Journal of Geophysical Research: Atmospheres*, *125*, e2019JD031982. https://doi.org/10.1029/2019JD031982

Chen, H., Wang, S., Wang, Y., & Zhu, J. (2020). Probabilistic projections of hydrological droughts through convection-permitting climate simulations and multi-model hydrological predictions. *Journal of Geophysical Research: Atmospheres*, *125*, e2020JD032914. https://doi.org/10.1029/2020JD032914

Christian, J., Christian, K., & Basara, J. B. (2015). Drought and pluvial dipole events within the great plains of the United States. *Journal of Applied Meteorology and Climatology*, *54*(9), 1886–1898. https://doi.org/10.1175/JAMC-D-15-0002.1

Darenova, E., Holub, P., Krupkova, L., & Pavelka, M. (2017). Effect of repeated spring drought and summer heavy rain on managed grassland biomass production and CO_2 efflux. *Journal of Plant Ecology*, *10*(3), 476–485. https://doi.org/10.1093/jpe/rtw058

Dong, X., Xi, B., Kennedy, A., Feng, Z., Entin, J. K., Houser, P. R., et al. (2011). Investigation of the 2006 drought and 2007 flood extremes at the Southern Great Plains through an integrative analysis of observations. *Journal of Geophysical Research*, *116*, D03204. https://doi.org/10.1029/2010JD014776

Du, J., Fang, J., Xu, W., & Shi, P. (2013). Analysis of dry/wet conditions using the standardized precipitation index and its potential usefulness for drought/flood monitoring in Hunan Province, China. *Stochastic Environmental Research and Risk Assessment*, *27*(2), 377–387. https://doi.org/10.1007/s00477-012-0589-6

Espinoza, J. C., Ronchail, J., Guyot, J. L., Junquas, C., Drapeau, G., Martinez, J. M., et al. (2012). From drought to flooding: Understanding the abrupt 2010-11 hydrological annual cycle in the Amazonas River and tributaries. *Environmental Research Letters*, *7*(2), 024008. https://doi.org/10.1088/1748-9326/7/2/024008

Feng, G. L., Yang, H. W., Zhang, S. X., Wang, K., & Shen, B. Z. (2012). A preliminary research on the reason of a sharp turn from drought to flood in the middle and lower reaches of the Yangtze River in late spring and early summer of 2011. *Chinese Journal of Atmospheric Sciences*, *36*(5), 1009–1026. https://doi.org/10.3878/j.issn.1006-9895.2012.11220 (in Chinese)

Feng, J., Yan, D., Li, C., Gao, Y., & Liu, J. (2014). Regional frequency analysis of extreme precipitation after drought events in the Heihe River Basin, Northwest China. *Journal of Hydrologic Engineering*, *19*(6), 1101–1112. https://doi.org/10.1061/(ASCE)HE.1943-5584.0000903

Giorgi, F., Coppola, E., Solmon, F., Mariotti, L., Sylla, M. B., Bi, X., et al. (2012). RegCM4: Model description and preliminary tests over multiple CORDEX domains. *Climate Research*, *52*(1), 7–29. https://doi.org/10.3354/cr01018

Giorgi, F., Im, E. S., Coppola, E., Diffenbaugh, N. S., Gao, X. J., Mariotti, L., & Shi, Y. (2011). Higher hydroclimatic intensity with global warming. *Journal of Climate*, *24*(20), 5309–5324. https://doi.org/10.1175/2011JCLI3979.1

Handwerger, A. L., Huang, M. H., Fielding, E. J., Booth, A. M., & Bürgmann, R. (2019). A shift from drought to extreme rainfall drives a stable landslide to catastrophic failure. *Scientific Reports*, *9*(1), 1–12. https://doi.org/10.1038/s41598-018-38300-0

Harris, I., Jones, P. D., Osborn, T. J., & Lister, D. H. (2014). Updated high-resolution grids of monthly climatic observations—The CRU TS3.10 dataset. *International Journal of Climatology*, *34*(3), 623–642. https://doi.org/10.1002/joc.3711

Harris, I., Osborn, T. J., Jones, P. D., & Lister, D. H. (2020). Version 4 of the CRU TS monthly high-resolution gridded multivariate climate dataset. *Scientific Data*, *7*(1), 1–18. https://doi.org/10.1038/s41597-020-0453-3

Hastenrath, S., Polzin, D., & Mutai, C. (2010). Diagnosing the droughts and floods in equatorial east Africa during boreal autumn 2005-08. *Journal of Climate*, *23*(3), 813–817. https://doi.org/10.1175/2009JCLI3094.1

He, X., & Sheffield, J. (2020). Lagged compound occurrence of droughts and pluvials globally over the past seven decades. *Geophysical Research Letters*, *47*, e2020GL087924. https://doi.org/10.1029/2020GL087924

Ji, Z., Li, N., & Wu, X. (2018). Threshold determination and hazard evaluation of the disaster about drought/flood sudden alternation in Huaihe River basin, China. *Theoretical and Applied Climatology*, *133*(3–4), 1279–1289. https://doi.org/10.1007/s00704-017-2257-8

Liu, Y., Zhu, Y., Ren, L., Singh, V. P., Yong, B., Jiang, S., et al. (2019). Understanding the spatiotemporal links between meteorological and hydrological droughts from a three-dimensional perspective. *Journal of Geophysical Research: Atmospheres*, *124*, 3090–3109. https://doi.org/10.1029/2018JD028947

Long, D., Shen, Y., Sun, A., Hong, Y., Longuevergne, L., Yang, Y., et al. (2014). Drought and flood monitoring for a large karst plateau in Southwest China using extended GRACE data. *Remote Sensing of Environment*, *155*, 145–160. https://doi.org/10.1016/j.rse.2014.08.006

Ma, Y., Yang, Y., & Wang, C. (2019). How essential of the balance between large and small scale features to reproduce precipitation during a sudden sharp turn from drought to flood. *Climate Dynamics*, *52*(7–8), 5013–5029. https://doi.org/10.1007/s00382-018-4445-3

Madakumbura, G. D., Kim, H., Utsumi, N., Shiogama, H., Fischer, E. M., Seland, Ø., et al. (2019). Event-to-event intensification of the hydrologic cycle from 1.5 °C to a 2 °C warmer world. *Scientific Reports*, *9*(1), 1–7. https://doi.org/10.1038/s41598-019-39936-2

Marquardt Collow, A. B., Bosilovich, M. G., & Koster, R. D. (2016). Large-scale influences on summertime extreme precipitation in the Northeastern United States. *Journal of Hydrometeorology*, *17*(12), 3045–3061. https://doi.org/10.1175/JHM-D-16-0091.1

McKee, T. B., Doesken, N. J., & Kliest, J. (1993). The relationship of drought frequency and duration to time scales. In proceedings of the 8th conference of applied climatology, 17–22 January, Anaheim, CA. In *Eighth Conference on Applied Climatology* (pp. 17–22). California.

Qing, Y., Wang, S., Zhang, B., & Wang, Y. (2020). Ultra-high resolution regional climate projections for assessing changes in hydrological extremes and underlying uncertainties. *Climate Dynamics*, *55*(7–8), 2031–2051. https://doi.org/10.1007/s00382-020-05372-6

Schaub, S., & Finger, R. (2020). Effects of drought on hay and feed grain prices. *Environmental Research Letters*, *15*(3). https://doi.org/10.1088/1748-9326/ab68ab

Shan, L., Zhang, L., Song, J., Zhang, Y., She, D., & Xia, J. (2018). Characteristics of dry-wet abrupt alternation events in the middle and lower reaches of the Yangtze River Basin and the relationship with ENSO. *Journal of Geographical Sciences*, *28*(8), 1039–1058. https://doi.org/10.1007/s11442-018-1540-7

Singh, D., Tsiang, M., Rajaratnam, B., & Diffenbaugh, N. S. (2014). Observed changes in extreme wet and dry spells during the south Asian summer monsoon season. *Nature Climate Change*, *4*(6), 456–461. https://doi.org/10.1038/nclimate2208

Su, B., Huang, J., Fischer, T., Wang, Y., Kundzewicz, Z. W., Zhai, J., et al. (2018). Drought losses in China might double between the 1.5°C and 2.0°C warming. *Proceedings of the National Academy of Sciences of the United States of America*, *115*(42), 10,600–10,605. https://doi.org/10.1073/pnas.1802129115

Swain, D. L., Langenbrunner, B., Neelin, J. D., & Hall, A. (2018). Increasing precipitation volatility in twenty-first-century California. *Nature Climate Change*, *8*(5), 427–433. https://doi.org/10.1038/s41558-018-0140-y

Tang, J., Niu, X., Wang, S., Gao, H., Wang, X., & Wu, J. (2016). Statistical downscaling and dynamical downscaling of regional climate in China: Present climate evaluations and future climate projections. *Journal of Geophysical Research: Atmospheres*, *121*, 2110–2129. https://doi.org/10.1002/2015JD023977

Vicente-Serrano, S. M., Beguería, S., & López-Moreno, J. I. (2010). A multiscalar drought index sensitive to global warming: The standardized precipitation evapotranspiration index. *Journal of Climate*, *23*(7), 1696–1718. https://doi.org/10.1175/2009JCLI2909.1

Vido, J., Nalevanková, P., Valach, J., Šustek, Z., & Tadesse, T. (2019). Drought analyses of the Horné Požitavie region (Slovakia) in the period 1966-2013. *Advances in Meteorology*, *2019*, 16–18. https://doi.org/10.1155/2019/3576285

Wang, G., Wang, D., Trenberth, K. E., Erfanian, A., Yu, M., Bosilovich, M. G., & Parr, D. T. (2017). The peak structure and future changes of the relationships between extreme precipitation and temperature. *Nature Climate Change*, *7*(4), 268–274. https://doi.org/10.1038/nclimate3239

Wang, J., Xiao, H., Hartmann, R., & Yue, Y. (2014). Physical geography of China and the U.S. In *A comparative geography of China and the U. S* (pp. 23–81). Dordrecht: Springer. https://doi.org/10.1007/978-94-017-8792-5_2

Wang, L., & Gu, W. (2016). The Eastern China flood of June 2015 and its causes. *Science Bulletin*, *61*(2), 178–184. https://doi.org/10.1007/s11434-015-0967-9

Wang, S., Ancell, B., Huang, G., & Baetz, B. (2018). Improving robustness of hydrologic ensemble predictions through probabilistic pre-and post-processing in sequential data assimilation. *Water Resources Research*, *54*, 2129–2151. https://doi.org/10.1002/2018WR022546

Wang, S., Tian, H., Ding, X. J., Xie, W. S., & Tao, Y. (2009). Climate characteristics of precipitation and phenomenon of drought-flood abrupt alternation during main flood season in Huaihe River Basin. *Chinese Journal of Agrometeorology*, *30*(1), 31–34. (in Chinese)

Wang, S., & Wang, Y. (2019). Improving probabilistic hydroclimatic projections through high-resolution convection-permitting climate modeling and Markov chain Monte Carlo simulations. *Climate Dynamics*, *53*(3–4), 1613–1636. https://doi.org/10.1007/s00382-019-04702-7

Wilson, W., Hassell, D., Hein, D., Wang, C., Tucker, S., Jones, R., & Taylor, R. (2015). Technical manual for PRECIS: The met office hadley centre regional climate modelling system version 2.0. 0.

Wu, Z., Li, J., He, J., & Jiang, Z. (2006). Occurrence of droughts and floods during the normal summer monsoons in the mid- and lower reaches of the Yangtze River. *Geophysical Research Letters*, *33*, L05813. https://doi.org/10.1029/2005GL024487

Xu, J., Wang, D., Qiu, X., Zeng, Y., Zhu, X., Li, M., et al. (2020). Dominant factor of dry-wet change in China since 1960s. *International Journal of Climatology*, 1–17. https://doi.org/10.1002/joc.6728

Yan, D. H., Wu, D., Huang, R., Wang, L. N., & Yang, G. Y. (2013). Drought evolution characteristics and precipitation intensity changes during alternating dry-wet changes in the Huang-Huai-Hai River basin. *Hydrology and Earth System Sciences*, *17*(7), 2859–2871. https://doi.org/10.5194/hess-17-2859-2013

Yang, L., Lam, J. C., & Tsang, C. L. (2008). Energy performance of building envelopes in different climate zones in China. *Applied Energy*, *85*(9), 800–817. https://doi.org/10.1016/j.apenergy.2007.11.002

Yatagai, A., Kamiguchi, K., Arakawa, O., Hamada, A., Yasutomi, N., & Kitoh, A. (2012). Aphrodite constructing a long-term daily gridded precipitation dataset for Asia based on a dense network of rain gauges. *Bulletin of the American Meteorological Society*, *93*(9), 1401–1415. https://doi.org/10.1175/BAMS-D-11-00122.1

Yoon, J. H., Wang, S. Y. S., Lo, M. H., & Wu, W. Y. (2018). Concurrent increases in wet and dry extremes projected in Texas and combined effects on groundwater. *Environmental Research Letters*, *13*(5). https://doi.org/10.1088/1748-9326/aab96b

Yu, M., Li, Q., Hayes, M. J., Svoboda, M. D., & Heim, R. R. (2014). Are droughts becoming more frequent or severe in China based on the standardized precipitation evapotranspiration index: 1951-2010? *International Journal of Climatology*, *34*(3), 545–558. https://doi.org/10.1002/joc.3701

Zhang, B., Wang, S., & Wang, Y. (2019). Copula-based convection-permitting projections of future changes in multivariate drought characteristics. *Journal of Geophysical Research: Atmospheres*, *124*, 7460–7483. https://doi.org/10.1029/2019JD030686

Zhang, B., Wang, S., & Zhu, J. (2020). A two-stage Bayesian multi-model framework for improving multidimensional drought risk projections over China. *Hydrology and Earth System Sciences Discussions*. https://doi.org/10.5194/hess-2020-247

Zhang, Y., Jiang, F., Wei, W., Liu, M., Wang, W., Bai, L., et al. (2012). Changes in annual maximum number of consecutive dry and wet days during 1961-2008 in Xinjiang, China. *Natural Hazards and Earth System Sciences*, *12*(5), 1353–1365. https://doi.org/10.5194/nhess-12-1353-2012

Zhao, J., Xia, H., Yue, Q., & Wang, Z. (2020). Spatiotemporal variation in reference evapotranspiration and its contributing climatic factors in China under future scenarios. *International Journal of Climatology*, *40*(8), 3813–3831. https://doi.org/10.1002/joc.6429

Zhu, J., Wang, S., & Huang, G. (2019). Assessing climate change impacts on human-perceived temperature extremes and underlying uncertainties. *Journal of Geophysical Research: Atmospheres*, *124*, 3800–3821. https://doi.org/10.1029/2018JD029444

Zong, Y., & Chen, X. (2000). The 1998 flood on the Yangtze, China. *Natural Hazards*, *22*(2), 165–184. https://doi.org/10.1023/A:1008119805106

Zotarelli, L., & Dukes, M. (2010). Step by step calculation of the Penman-Monteith evapotranspiration (FAO-56 method). *Institute of Food and Agricultural Sciences*, 1–10. https://edis.ifas.ufl.edu/pdffiles/AE/AE45900.pdf